DOI: 10.1111/gcb.16683

RESEARCH ARTICLE



Check for updates

Satellite solar-induced chlorophyll fluorescence tracks physiological drought stress development during 2020 southwest US drought

Yao Zhang^{1,2} | Jianing Fang^{1,3} | William Kolby Smith⁴ | Xian Wang⁴ | Pierre Gentine³ | Russell L. Scott⁵ | Mirco Migliavacca⁶ | Sujong Jeong⁷ | Marcy Litvak⁸ 5 | Sha Zhou⁹

Correspondence

Yao Zhang, Sino-French Institute for Earth System Science, College of Urban and Environmental Sciences, Peking University, Beijing, China. Email: zhangyao@pku.edu.cn

Funding information

National Natural Science Foundation of China, Grant/Award Number: 42141005: NASA Carbon Cycle Science Program. Grant/Award Number: 80NSSC23K0109

Abstract

Monitoring and estimating drought impact on plant physiological processes over large regions remains a major challenge for remote sensing and land surface modeling, with important implications for understanding plant mortality mechanisms and predicting the climate change impact on terrestrial carbon and water cycles. The Orbiting Carbon Observatory 3 (OCO-3), with its unique diurnal observing capability, offers a new opportunity to track drought stress on plant physiology. Using radiative transfer and machine learning modeling, we derive a metric of afternoon photosynthetic depression from OCO-3 solar-induced chlorophyll fluorescence (SIF) as an indicator of plant physiological drought stress. This unique diurnal signal enables a spatially explicit mapping of plants' physiological response to drought. Using OCO-3 observations, we detect a widespread increasing drought stress during the 2020 southwest US drought. Although the physiological drought stress is largely related to the vapor pressure deficit (VPD), our results suggest that plants' sensitivity to VPD increases as the drought intensifies and VPD sensitivity develops differently for shrublands and grasslands. Our findings highlight the potential of using diurnal satellite SIF observations to advance the mechanistic understanding of drought impact on terrestrial ecosystems and to improve land surface modeling.

KEYWORDS

afternoon depression, diurnal variation, OCO-3, photosynthesis, SIF, stomatal conductance

¹Sino-French Institute for Earth System Science, College of Urban and Environmental Sciences, Peking University, Beijing, China

²Institute of Carbon Neutrality, Peking University, Beijing, China

³Department of Earth and Environmental Engineering, Columbia University, New York, New York, USA

⁴School of Natural Resources and the Environment, University of Arizona, Tucson, Arizona, USA

⁵Southwest Watershed Research Center, USDA Agricultural Research Service, Tucson, Arizona, USA

⁶European Commission, Joint Research Centre, Ispra, Italy

⁷Department of Environmental Planning, Graduate School of Environmental Studies, Seoul National University, Seoul, South Korea

⁸Department of Biology, University of New Mexico, Albuquerque, New Mexico, USA

⁹State Key Laboratory of Earth Surface Processes and Resources Ecology, Faculty of Geographical Science, Beijing Normal University, Beijing, China

1 | INTRODUCTION

Drought frequency and severity are projected to increase with global warming, leading to worldwide forest mortality and significant reduction in terrestrial carbon uptake (Allen et al., 2010; Anderegg et al., 2013; Ciais et al., 2005; Dai, 2012). Large uncertainties still exist in modeling the impact of droughts on ecosystem function, limiting the accurate projections of the terrestrial biogeochemical and biophysical feedbacks in the future (McDowell et al., 2022; Trugman et al., 2018). Decades of satellite observations have provided valuable information on drought-induced canopy structural changes (Liu et al., 2020; Zhang et al., 2021). However, the impact of drought stress on plant physiology is not well characterized by traditional optical remote sensing (Zhang et al., 2016). Such information would not only support drought early warning systems, for example, to identify the so-called "point of no return", which is a drought phase when physiological drought stress accumulates and causes irreversible damage to an organ or the entire plant (McDowell et al., 2022), but it could also help improve the modeling of photosynthesis and evapotranspiration at large scale (Martens et al., 2017; Stocker et al., 2019).

The successful retrieval of solar-induced chlorophyll fluorescence (SIF) from satellite provides new opportunities to monitor physiological drought stress across large spatial scale (Frankenberg et al., 2011). SIF is the relatively small amount of energy emitted from the excited chlorophyll-a molecules during the light reaction of the photosynthesis process (Baker, 2008; Porcar-Castell et al., 2014). Like photosynthesis, SIF is affected not only by canopy structure and vegetation greenness, which determine vegetation light absorption, but also by physiological processes, which regulate the light harvest and electron transport chain (Adams & Demmig-Adams, 2004; Porcar-Castell et al., 2021). The fluorescence efficiency describes the efficiency at which photosystems convert the energy absorption to SIF emissions, a process strongly regulated by the physiological stress and has little canopy structural information. It is still challenging to derive such physiological information from satellite-retrieved SIF due to the large uncertainty in each individual SIF sounding (Sun et al., 2018), the complex radiative transfer that links leaf-level SIF emission and top of the atmosphere satellite observation (Yang & van der Tol, 2018), and the strong coupling between plant physiological and structural changes at weekly or monthly timescales at which most satellite SIF observations are obtained (Zhang et al., 2016).

The strong coupling between structural and physiological changes breaks down within a diurnal cycle because plants' stomata and metabolism respond more rapidly to drought stress than canopy structure (Xiao et al., 2021). Plant stomata operate nearly instantaneously in an effort to optimize carbon gains per unit water loss (Cowan & Farquhar, 1977; Lin et al., 2015; Zhou et al., 2014). This suggests that at diurnal time scale when soil water is limiting, stomatal conductance, leaf water potential and CO₂ metabolism will decrease with vapor pressure deficit (VPD), causing a strong decline of plant photosynthesis in the afternoon, a phenomenon known as afternoon depression (Franco & Lüttge, 2002). This decoupling between structural and physiological changes enables the use of

sub-daily observations of gas exchanges to understand the physiological response to dryness at eddy covariance (EC) flux tower sites (Novick, Ficklin, et al., 2016). However, such sub-daily information on vegetation physiological drought stress cannot be readily obtained contiguously at a global scale.

The Orbiting Carbon Observatory-3 (OCO-3), NASA's new instrument onboard the international space station (ISS), provides a unique opportunity to obtain the diurnal variation of SIF (Taylor et al., 2020). OCO-3 is launched in May 2019. Similar to OCO-2, it is designed to measure the column concentration of trace gases in the atmosphere (Eldering et al., 2019). OCO-3 has ultra-high spectral resolutions at atmospheric absorption bands, allowing the SIF retrieval based on the Fraunhofer line filling mechanism. Previous spaceborne SIF observing platforms are all on sun-synchronous orbits, with limited capability to measure SIF at a fixed time of the day. Although their near-fixed local observing time allows for a direct comparison from day to day, it cannot provide dynamic information within a diurnal cycle, a time scale at which SIF and its physiological components all change considerably in response to stress. OCO-3 is on a low-inclination precessing orbit so that the overpass time for a given latitude changes through time, allowing it to sample all times of the day from dawn to dusk, with an illumination cycle of around 66 days. The diurnal changes of fluorescence efficiency can therefore be regarded as a good indicator of plant physiological responses to environmental stresses. Compared to other SIF satellites with wide swath and global coverage (such as GOME-2 or TROPOMI), the swath width for OCO-3 is only around 10km, with a single sounding footprint size of 1.6 km × 2.2 km. However, OCO-3 has a much higher spectral resolution and signal-to-noise ratio compare to other sensors, both of which are essential for obtaining high quality SIF signals (Taylor et al., 2020). These characteristics give us a unique opportunity to investigate the diurnal changes of the physiological responses of vegetation to environmental drivers.

In this study, we focus on the wide-spread, severe summer drought that happened in 2020 across the Southwestern US ("Southwest"), characterized by record-low precipitation and record-high air temperature and VPD (Dannenberg et al., 2022). Using radiative transfer and machine learning modeling, we demonstrate for the first time how OCO-3 SIF can be used to monitor the diurnal physiological stress across large spatial scales. This spatially explicit physiological information further reveals a biome-dependent drought stress development in 2020 Southwest drought.

2 | MATERIALS

We used SIF data from both satellite platforms (OCO-3, TROPOMI) and an in-situ observation site (US-Wkg) in this study. To derive and validate the physiological signals, we also used EC observations from nine sites located in southwest US, spectral reflectance measurements from both Moderate resolution Imaging Spectroradiometer (MODIS) and in-situ observations, landcover datasets, drought stress indicator from US drought monitor (USDM). Detailed information is described below.

2.1 | Satellite SIF dataset

We used OCO-3 SIF vEarly dataset provided by JPL (Taylor et al., 2020). OCO-3 has four observation modes on land, that is, the nadir mode, glint mode, target mode and snapshot area mapping mode (SAM; Figure S1). The SAM mode is unique for OCO-3, which allows for fine-scale spatial sampling over large area (around 85×85km). However, previous studies have demonstrated that SIF is strongly affected by the solar and viewing geometry (Zhang & Zhang, 2023; Zhang, Zhang, et al., 2018), which will complicate the interpretation of the diurnal variation of the SIF signal. Therefore, in this study, we only used the observations from the nadir mode to minimize the effect of viewing geometry.

One unique feature for OCO-3 is that SIF is observed at different time of the day, however, due to the characteristics of the ISS orbit, there is a large difference in the data acquisition timing for each month (Figure S2; Taylor et al., 2020). Even months (February, April, etc.) have much more observations which are evenly distributed throughout the day. Observations for odd months are much less and are mostly acquired in the early morning or late afternoon. Considering at a diurnal timescale, physiological stress is strongest in the early afternoon (Xiao et al., 2021). To increase the robustness of the results, we only used even months for the analysis.

We also used SIF retrievals from TROPOMI onboard the Sentinel-5P satellite (Köhler et al., 2018). TROPOMI SIF provides high spatial resolution ($7\times3.5\,\mathrm{km}$), spatially contiguous observations of the Earth surface since November, 2017. TROPOMI SIF is directly observed by the satellite, and should be able to capture the physiological drought stress. However, TROPOMI observations are obtained around 13:30 local time and do not provide diurnal SIF variation. We used TROPOMI SIF to demonstrate that the observed afternoon depression is not caused by spatial sampling biases of OCO-3.

2.2 | EC flux dataset

We used nine EC sites located in, or close to, our study area (Table S1). These sites were selected due to the data availability: each site must have observations for the entire year of 2020. These sites cover a large variety of biome types, including three evergreen needleleaf forest sites, two grassland sites, two woody savanna sites, one savanna site, and one open shrubland site. Here, we grouped the latter three biome types in a single class named shrublands. Considering that grassland and shrubland dominate the study area, these sites can generally represent the evolution of drought stress for the entire region.

We followed the standard protocol and used the R package "REddyProc" to process the EC data (Wutzler et al., 2018). We first checked the data quality for each month during 2016–2020. For each site-year, at least 10 out of 12months must have at least 50% valid net ecosystem exchange (NEE) measurement. We also extracted hourly "surface_solar_radiation_downwards" and "soil_temperature_level_2 (7–28cm)" from the ERA5 Land Hourly reanalysis dataset. The reanalysis dataset showed very good agreement with

the site level measurements, with mean correlation coefficients of 0.90 and 0.94 based on available radiation and soil temperature data, respectively. For those sites that have missing solar radiation or soil temperature observations, we filled 饿的 the gaps with ERA5.

The net ecosystem exchange (NEE) was first calculated as the flux of CO₂ and storage whenever possible. The gaps in NEE were then filled with the marginal distribution sampling method (Reichstein et al., 2005). We used both nighttime (Reichstein et al., 2005) and daytime (Lasslop et al., 2010) partitioning method to obtain the gross primary production (GPP) and ecosystem respiration. The difference between the two methods was generally small for the months with enough valid (not gap-filled) observations. But the nighttime method exhibited larger fluctuation in the afternoon especially when the ecosystem is under drought stress. To better demonstrate the diurnal variation of GPP and the afternoon depression, we used the estimates from daytime partitioning method throughout the study as suggested by a previous study (Martini et al., 2022).

2.3 | In-situ SIF observation

We used the SIF observations at Walnut Gulch Kendall grassland site (US-Wkg, 31.74°N, 109.94°W). This is a grassland site with warm winter and dry summer. The mean annual temperature is 15.64°C and the mean annual precipitation is 407 mm. The dominant species is Lehmann lovergrass (*Eragrostis lehmanniana* Nees), with small fraction of mesquite and shrub (Scott et al., 2010). The SIF was measured using a FluoSpec2 system mounted on a tower roughly 7-m above the surface (Yang, Shi, et al., 2018). The FluoSpec2 system used two optical fibers connecting to an ultra-high spectral resolution spectrometer (QE-Pro, Ocean Optics, Inc). These two optical fibers faced upwards and downwards to measure the irradiance and radiance, respectively. Both fibers were attached to a cosine corrector to get a nearly 170° field of view. The other end of optical fibers was attached to an inline shutter, which allowed the spectrometer to measure the irradiance or radiance once at a time.

Radiometric and wavelength calibrations were performed at the begin and one time during the field campaign using a radiometric calibration light source (LS-1-CAL, OceanOptics, Inc.) and a wavelength calibration light source (HG-1, OceanOptics, Inc.). The derived radiometric and wavelength calibration factors were used to convert the raw digital number data collected by the spectrometer to irradiance and radiance between 680nm and 775nm. The system continuously measured irradiance and radiance during the daytime, from which SIF was retrieved at a half-hour timestep using the spectral fitting method at 760 nm (Meroni et al., 2010). We filtered all SIF retrievals during cloudy conditions when PAR observed was <75% of top-of-atmosphere PAR (based on solar zenith angle), and when SIF < 0 mW m⁻² nm⁻¹ sr⁻¹ due to a change in the light environment during the upward and downward facing measurements. We additionally filtered SIF retrievals during periods of low solar zenith angle before 8:30 and after 16:00 local time. Surface reflectance was also measured at the site using Spectral Reflectance Sensors (SRS, Decagon Devices) installed at the same location and height as FluoSpec2, from which Normalized Difference

Vegetation Index (NDVI) was calculated. The sensor retrieved NDVI showed good seasonal dynamics very consistent with MODIS NDVI but with an offset. We used MODIS NDVI to correct this bias to derive a consistent diurnal NDVI signal at the site.

2.4 Other datasets

We used 500 m daily MODIS Nadir BRDF-adjusted reflectance data-set (NBAR, MCD43A4) band 1–4 (red, near infrared, blue, green) to derive the physiological drought stress based on a deep learning approach (Schaaf & Wang, 2015). For each SIF retrieval (sounding), we generated a polygon for its footprint $(1.6 \times 2.25 \, \text{km})$ using the corner coordinates and retrieve the average reflectance for each of the four NBAR band. In total, we retrieved NBAR reflectance for 4.17 million OCO-3 SIF soundings using the Google Earth Engine. We also calculated the NDVI from the NBAR reflectance.

United States drought monitor (USDM) is a knowledge-based drought classification system that provides weekly drought intensity monitoring for the entire US. Drought is classified into four categories (moderate, severe, extreme, and exceptional) based on a suite of drought indices (including Palmer Drought Severity Index, Standardized Precipitation Index, etc.) and experts and a network of observers across the country. It is a comprehensive and integrated drought assessment. We used the spatial maps and the areal summary of this dataset as an indicator of drought stress. We also used MODIS land surface temperature from MYD11C1 as an indirect indicator of drought stress and MODIS land cover dataset from MCD12C1 to classify the SIF soundings into different biome types.

3 | METHODS

We used both a radiative transfer modeling method and a deep learning model to derive the afternoon depression signal from the satellite SIF observations. For the radiative modeling method, we derived and compared the ratio between afternoon and morning fluorescence efficiency as afternoon depression. For the deep learning model, we trained a residual network to predict a potential non-drought SIF mostly based on the canopy structure information. The physiological stress would be expressed as the difference between observed SIF and this potential non-drought SIF.

3.1 | Estimating fluorescence yield using radiative transfer modeling

Satellite SIF observations can be expressed as the product of incident photosynthetic active radiation (PAR), fraction of PAR absorbed by chlorophyll pigments (fPAR), fluorescence efficiency (ϕ_f) and the escape probability ($f_{\rm esc}$) from leaf level to the top of canopy:

$$SIF = PAR \times fPAR \times \phi_f \times f_{esc}$$
 (1)

Following (Zeng et al., 2019), the escape probability can be calculated as:

$$f_{\rm esc} = \frac{\rm NIR_{\rm V}}{\rm fPAR} = \frac{(\rm NDVI - \it a) \times \rho_{\rm NIR}}{\rm fPAR} \tag{2}$$

where ρ_{NIR} is the reflectance at the near-infrared (NIR) band and a is a factor to account for the soil background. We set a to 0.1 in this study, as shown by a comparison between SIF and NDVI. Combining Equation (1) and Equation (2)

$$\phi_{\rm f} = \frac{{\sf SIF}}{{\sf PAR} \times ({\sf NDVI} - a) \times \rho_{\sf NIR}} \approx \frac{{\sf SIF}_{\sf relative}}{{\sf NDVI} - a} \tag{3}$$

where

$$SIF_{relative} = \frac{SIF}{L_{NIP}} \tag{4}$$

 $L_{\rm NIR}$ is surface radiance at NIR band can be directly obtained from concurrent OCO-3 observations as the continuum radiance at 740 nm. Since SIF and $L_{\rm NIR}$ have the same unit, and SIF_{relative} and ϕ_f calculated here are unitless, the absolute value of ϕ_f is not directly comparable with other studies which uses PAR and $\rho_{\rm NIR}$. The advantage is that, our approach does not need to consider the complex radiative transfer in the canopy, and the varying PAR conditions at the satellite overpass. It should be noted that ϕ_f is also affected by PAR, however, this effect is not considered in our study since the effect size is mostly small when PAR is large (van der Tol et al., 2014).

 ϕ_f can be directly calculated using Equation (3). However, in practice, we used the regression slope between SIF_{relative} and NDVI -a as ϕ_f . This can reduce the large uncertainties when NDVI -a is close to zero. $L_{\rm NIR}$ is usually large and very accurately measured, therefore, the uncertainties in SIF_{relative} mostly come from SIF retrievals and are not affected by the calculation using Equation (4).

Similarly, vegetation photosynthesis can also be expressed as a function of PAR, fPAR and photochemistry efficiency (ϕ_n) :

$$\mathsf{GPP} = \mathsf{PAR} \times \mathsf{fPAR} \times \phi_{p}. \tag{5}$$

 ϕ_p can be derived as the regression slope between GPP and PAR×fPAR:

$$\phi_p = \frac{\mathsf{GPP}}{\mathsf{PAR}} \times \frac{1}{\mathsf{fPAR}}.\tag{6}$$

To avoid the uncertainties introduced by the estimates of fPAR for each EC flux site, we calculated $\phi_p \times \text{fPAR}$ which only relies on tower measured GPP and PAR. Unlike photochemistry efficiency (ϕ_p) that shows a strong light saturation at a diurnal time scale, ϕ_f have limited variation under varying light conditions (Yang, Ryu, et al., 2018). However, with increasing drought stress, both ϕ_p and ϕ_f will decrease while extra energy will dissipate as heat (Porcar-Castell et al., 2014). To capture the diurnal variation of the ϕ_f and make it comparable with the ϕ_p in response to drought stress, we

We used a batch size of 512, learning rate of 0.002 and number of epochs of 200 to train the ResNet, we also used early stopping as the regularization to reduce overfitting. The ResNet shows acceptable performance, considering the large uncertainty in the individual SIF retrieval (Figures S4-S6). We also designed an experiment to demonstrate that the ResNet performance is similar to the "optimal model" given the low signal-to-noise ratio (see details in Data S1 and Figure S7). Since this ResNet was trained on non-drought SIF observations, it should be able to capture the general relationship between SIF and vegetation status, climate, and observation time but not the water stress impact. Comparing this predicted reference SIF to the actual OCO-3 SIF data would thus undercover the stress dependence.

Using these two trained ResNet, we predicted the SIF values for the Southwest during 2020, and this predicted SIF should be considered as non-drought stressed SIF. The difference between the OCO-3 observed SIF and predicted ones (Δ SIF) should be interpreted as the drought induced SIF declines across different time of the day. Considering the large uncertainty in each individual SIF retrieval, we used the average of Δ SIF within the 0.05-degree radius to reduce the noise.

calculated the regression slope between SIF_{relative} and NDVI – a for morning (before 11:30 local time) and afternoon (after 13:30 local time) separately. Considering the symmetric shape of radiation for the two periods, the regression slopes should be equal for morning and afternoon if no stress presents. Similarly, $\phi_p \times \text{fPAR}$ can also be calculated for morning and afternoon separately. Within a diurnal cycle, the variations in fPAR are relatively small and symmetric for morning and afternoon. Therefore, the comparison between morning and afternoon ϕ_n can also be approximated by the morning and afternoon $\phi_n \times \text{fPAR}$, that is, the regression slopes between GPP and PAR. We estimated the regression slope and the 95% confidence intervals using the ordinary least square method. We did not consider the uncertainty in each individual SIF sounding since it can be greatly reduced after averaging over multiple observations. When drought stress presents and afternoon depression becomes stronger, both regression slopes for GPP and PAR, and $SIF_{relative}$ and NDVI - a will be smaller in the afternoon than in the morning. This difference in regression slopes can be regarded as an indicator of afternoon depression and the strength of physiological drought stress.

We did not directly compare the fluorescence efficiency for the early morning or late afternoon with that for the midday. Although this comparison may exhibit stronger afternoon depression signals, it also suffers from issues such as reduced numbers of samples for the regression and large differences in the solar zenith angle and canopy radiative transfer (Chang et al., 2021), which could bias the calculation of the ϕ_f and ϕ_p . Zeng's method for calculating the escape probability (f_{esc}) depends on an assumption of dark soil, that is, radiation that passes through the canopy will be fully absorbed by the soil. This is highly unlikely for our study area where vegetation is sparse and the soil background is bright. Our approach of comparing the regression slopes between morning and afternoon can eliminate this effect through normalization.

3.2 Deep learning predictions

The physiological drought stress will down-regulate SIF from its expected value when drought is not present. We used a deep learning approach (residual network, ResNet) to predict this expected non-drought SIF (SIF $_{\rm pred}$) value, and calculated the difference between the OCO-3 observed SIF and SIF $_{\mathrm{pred}}$ (Δ SIF) as an indicator of physiological drought stress (Figure S3). We assume the ResNet can capture the sun-sensor geometry effect, allowing us investigate the diurnal changes of Δ SIF. ResNet is a type of deep neural network which helps solve the degradation problem through shortcut connections, that is, the output of a shallower layer is directly added to the output of a deeper layer before applying the activation function. We built a ResNet with five shortcut blocks, with each block having two layers and 30 nodes for each layer. We used 14 variables as the input for the ResNet, including five related to the vegetation optical properties, that is, nadir BRDF-adjusted reflectance band 1-4 (corresponding to red, near infrared, blue, green band), and NDVI; four related to the local climate and environment (relative humidity, air temperature, downward shortwave radiation, altitude);

RESULTS

Impact of 2020 Southwest drought on terrestrial ecosystem

Starting in the summer of 2020, the Southwest has experienced a record-breaking extreme drought event (Dannenberg et al., 2022). According to the US Drought Monitor, the drought started in Utah and Colorado in May and June and rapidly expands through August and September, affecting the entire Southwest (Figure 1a; Figure S8). During this period, our study area, which is dominated by grassland and open shrubland (41.4% and 34.0%, respectively based on MODIS land cover map), exhibits strong positive land surface temperature anomalies in the early afternoon (circa 13:30, 5.4 ± 1.8 °C) compared to normal years based on observations from MODIS (Figure 1b,c) and EC flux towers (Figure S9). Both OCO-3 SIF and MODIS NDVI show lower values in the center of our study region

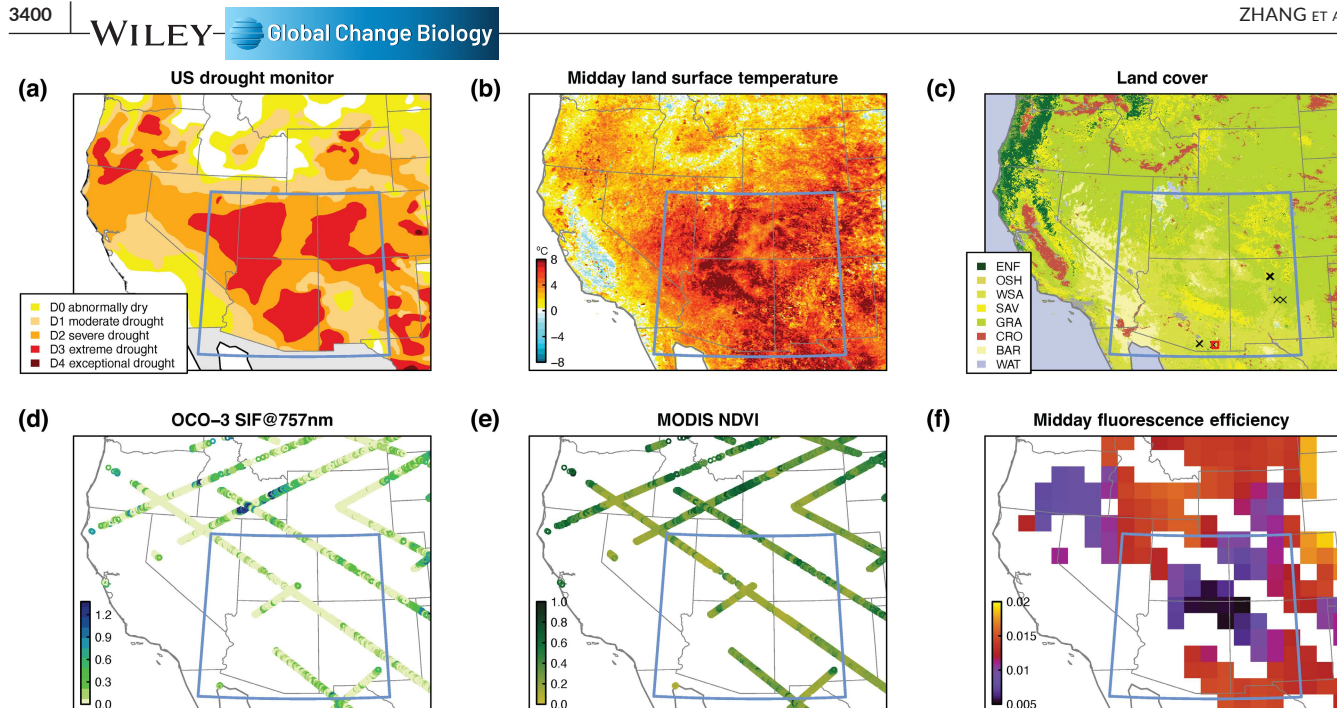


FIGURE 1 2020 Drought in US Southwest. (a) Drought categories from US Drought Monitor for the week of August 25, 2020. The blue rectangle shows the study area. (b) Midday land surface temperature (LST) anomaly for August. The anomaly is calculated using LST for 2020 minus multi-year average during 2010-2019. (c) Land cover map from MODIS for year 2019. The black cross signs indicate the eddy covariance (EC) flux tower sites used in this study. Red square indicates the EC site where site-level solar-induced chlorophyll fluorescence (SIF) observation is available. (d) Midday Orbiting Carbon Observatory 3 (OCO-3) SIF at 757 nm in 2020 August. The unit is mW m⁻² nm⁻¹ sr⁻¹. To reduce the uncertainty in SIF retrievals, the average value within a small neighboring area $(0.1^{\circ} \times 0.1^{\circ})$ is used for each sounding. (e) The MODIS NDVI for the corresponding OCO-3 soundings. (f) Midday fluorescence efficiency calculated from OCO-3 and MODIS as the regression slope between relative SIF and NDVI. The individual OCO-3 soundings are aggregated to 1°×1° gridcells. [Colour figure can be viewed at wileyonlinelibrary.com]

(Figure 1d,e). With radiative transfer modeling, we delineated the physiological information embedded in the SIF signal, represented by the fluorescence efficiency (Figure 1f). The spatial patterns of the fluorescence efficiency generally match the drought intensity and land surface temperature anomalies (Pearson's r=-.37 and -.24, p < .01), with the lowest values in the central part of the study region (Figure 1b,f; Figure S10). This spatial pattern from OCO-3 is also similar with that calculated from TROPOMI SIF (Figure S11), demonstrating the potential of using satellite datasets to understand plant physiological changes in response to drought. But such a spatial pattern may have large uncertainty due to the inaccurate characterization of structural information using vegetation indices. A more

robust estimate of the physiological signal should be acquired at diurnal time scales when structural and physiological processes decouple (Martini et al., 2022).

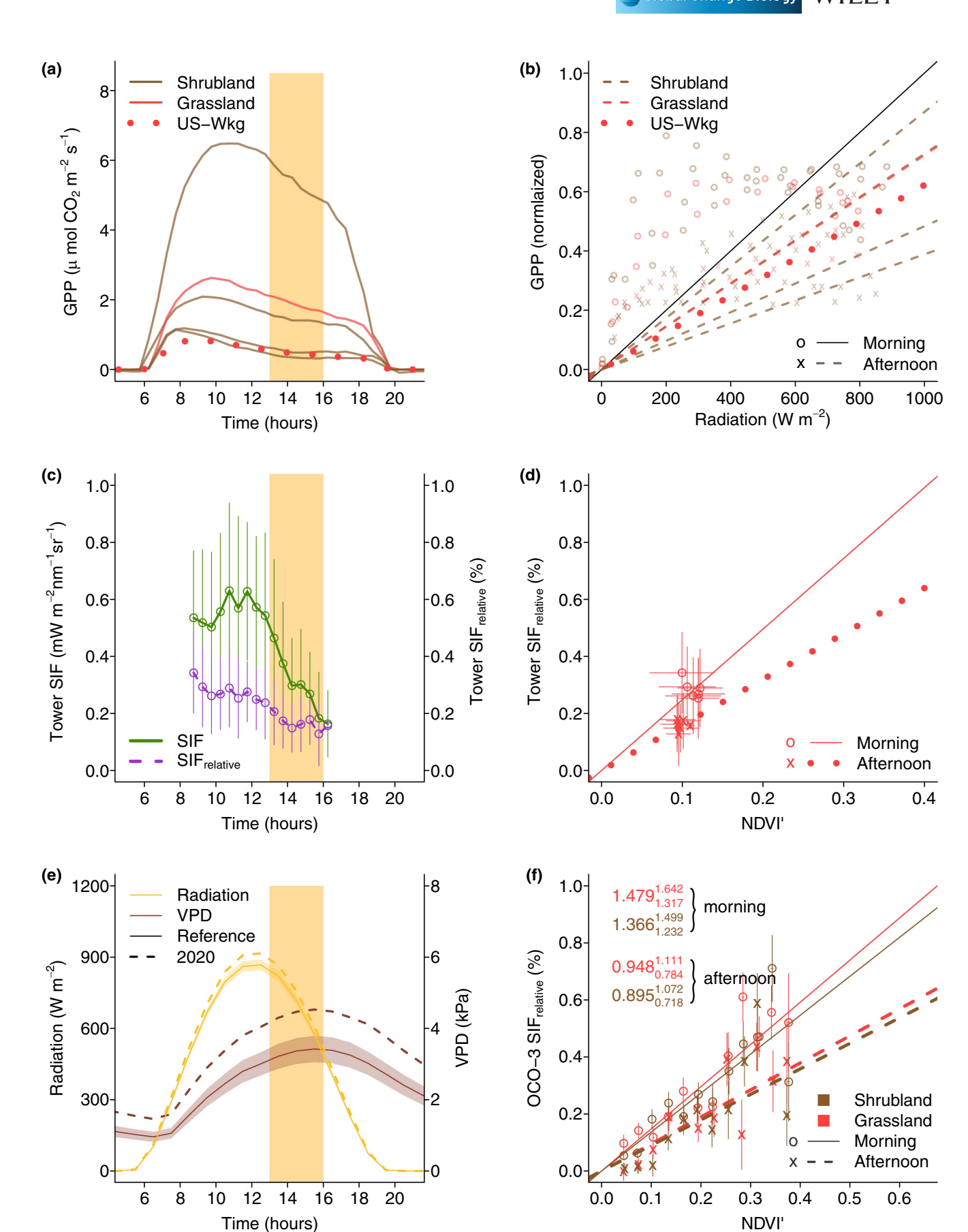
Afternoon depression as an indicator for physiological drought stress

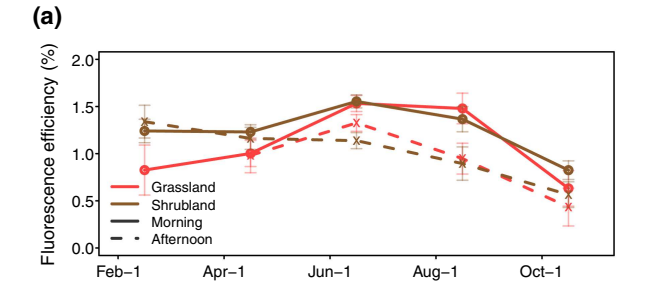
Using in-situ Ameriflux EC observations from nine sites in the Southwest (Figure 1c), we examine the monthly average diurnal variations of gross primary production (GPP) during the middle of the drought in August, 2020. In the absence of water limitation, we

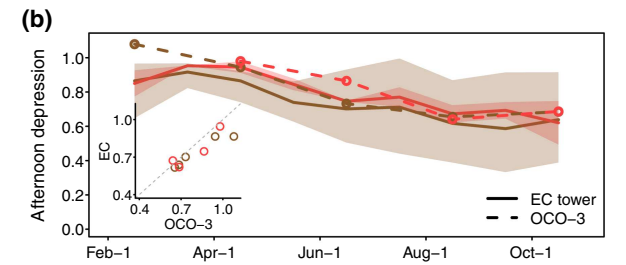
FIGURE 2 Afternoon depression at eddy covariance flux towers and with OCO-3 SIF. (a) The diurnal course of monthly mean gross primary production (GPP) at 6 grassland and shrubland flux tower sites in the study region for August, 2020. The locations of the sites are shown in Figure 1(c). Yellow shades indicate the period with strongest afternoon depression. (b) The relationship between GPP and solar radiation using the monthly average GPP and radiation for each time of the day. Regressions are conducted for the morning and afternoon observations, respectively. We use a scaling factor on GPP for each site each month so that the morning regression slope always equal to 1/1000, allowing the morning afternoon differences to be directly comparable across sites. Dotted lines in (a) and (b) indicate the observations from the Walnut Gulch Kendall grassland (US-Wkg) where SIF observations are available. (c) Diurnal variations of SIF and relative SIF at the US-Wkg site during August and September in 2020. (d) Fluorescence efficiency calculated at the US-Wkg site. (e) Diurnal course of the radiation and vapor pressure deficit for August for both 2020 and the reference period during 2010-2019 for the entire study region from ERA5. Shades indicate the 1 SD of the variation, (f) Fluorescence efficiency calculated from OCO-3 for grasslands and shrublands. Solid and dashed lines indicate the regressions for morning and afternoon soundings, respectively. Average fluorescence efficiency is calculated for each NDVI bin, with the error bar indicate the standard error of the mean. Regression slopes with 95% confidence intervals are shown in the top-left corner for both biome types. NDVI' is the NDVI adjusted for the soil background. [Colour figure can be viewed at wileyonlinelibrary.com]

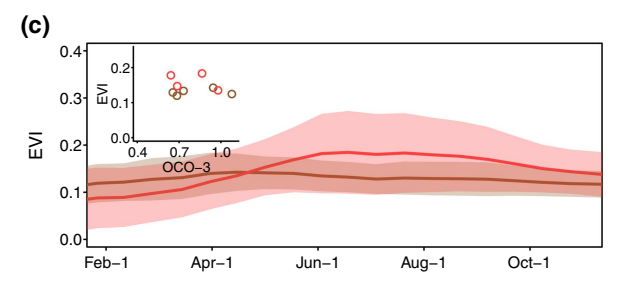
13652486, 2023, 12, Downloaded from https://online.library.wiley.com/doi/10.1111/gcb.16683 by University Of New Mexico, Wiley Online Library on [29/05/2024]. See the Terms

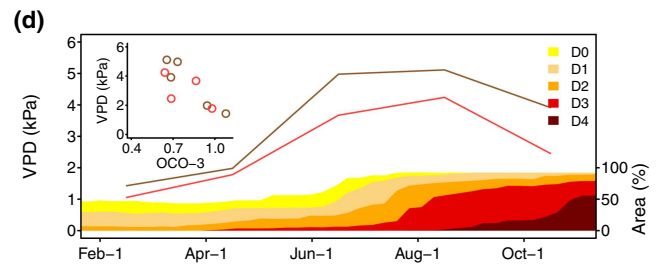
ditions) on Wiley Online Library for rules of use; OA articles are governed by the applicable Creative Commons Licens











expect that GPP would follow the incoming solar radiation and exhibit a nearly symmetrical diurnal pattern (Matthews et al., 2017). However, we observe large GPP declines in the afternoon, compared to the morning for most sites (Figure 2a). This corresponds to a decrease in light use efficiency (LUE, GPP divided by solar radiation) in the afternoon as the stomata partially close to prevent water losses, with average afternoon LUE reducing to only 67.3% and 61.7% of its morning values for grasslands and shrublands, respectively (Figure 2b). Forests exhibit little changes since they are mostly located in more mountainous regions with higher water availability (Figure S12), lower temperature and VPD, and are less affected by the drought (Knowles et al., 2020).

Using the in-situ SIF observations from the Walnut Gulch Kendall grassland site, we find the fluorescence efficiency also shows an evident depression in the afternoon (Figure 2c,d). The magnitude of the decline for fluorescence efficiency (35.5%) is close to the decline for LUE (37.8%). Both are much stronger than their counterpart in the same month but in a non-drought year (Figure S13). The morning-afternoon difference in both SIF and GPP can be used to indicate diurnal changes of vegetation physiological stress. But can we derive

FIGURE 3 Drought development and changes in afternoon depression. (a) Changes in morning and afternoon fluorescence efficiency for grassland and shrubland, with the error bars showing the 95% confidence interval. February afternoon estimates for grassland exhibit large uncertainty due to limited observations and are not shown here (Figure 2). (b) The afternoon depression of light use efficiency from eddy covariance (EC) towers and of fluorescence efficiency from OCO-3. The depression is calculated as the ratio of efficiencies between afternoon and morning for each month. The shades show the range of the depression from individual sites within each biome type. The inset shows the comparison of the depression derived from OCO-3 and EC. (c) The seasonal variation of enhanced vegetation index (EVI) for the grassland and shrubland in the study region. The shades show the standard deviation of the spatial variations. The inset show the comparison between the afternoon depression derived from OCO-3 and EVI. (d) The evolution of vapor pressure deficit for OCO-3 soundings (grassland and shrubland) and the drought classification for the entire study area using US drought monitor. D0 to D4 indicate abnormally dry, moderate drought, severe drought, extreme drought, exceptional drought, respectively. The inset shows the comparison between the afternoon depression estimated from OCO-3 and the vapor pressure deficit for the 5 months. [Colour figure can be viewed at wileyonlinelibrary.com]

such a diurnal physiological signal from satellite observations so that the stress can be monitored at large scale?

Although OCO-3 observes the Earth's surface at different time of the day, it is not possible to obtain both morning and afternoon SIF at the exact same locations due to the sparse swath-based sampling strategy (Figures S1 and S2). The diurnal variation of sunsensor geometry also affects the radiation absorption, making the fluorescence efficiency calculated at different times of the day not directly comparable (Chang et al., 2021). We therefore divide the observations into morning and afternoon considering the symmetrical solar zenith angle and the large differences in VPD between these two periods (Figure 2e). We find with this approach that the fluorescence efficiency is 35.9% and 34.5% lower in the afternoon than morning for grassland and shrubland, respectively (Figure 2f). This OCO-3 SIF derived afternoon depression, similar to the depression observed at the EC sites, provides robust evidence that OCO-3 captures the diurnal physiological drought stress.

4.3 | Temporal development of physiological drought stress

With this analysis framework, we evaluated the diurnal physiological stress changes during the entire drought period. Due to the limited observations of OCO-3 SIF in odd numbered months (Figure S2), we only retrieved morning and afternoon fluorescence efficiency for the five even months from February to October. Both grasslands and shrublands show similar seasonal patterns, with fluorescence efficiency slightly increasing from February to June (Figure 3a; Figures S14 and S15). Grasslands, compared to shrublands, show stronger increases, possibly due to a greater relief of cold stress as

they are mostly distributed in the northern part of the study area. Since June, fluorescence efficiency for both grasslands and shrublands started to decrease, with a large reduction in October, consistent with a rapid expansion of the extreme drought area (Figure 3d; Figure S8). Fluorescence efficiency is always lower in the afternoon than morning, and this difference increases as the drought develops.

We further quantify the strength of afternoon depression from both EC calculated LUE and OCO-3 derived fluorescence efficiency. The afternoon depression, calculated using either method, decline as the drought progresses since April, with a similar trend for both shrublands and grasslands (Figure 3b; Figure S12). In comparison, the absolute values of fluorescence efficiency mostly increase during this period. This suggests that changes of fluorescence efficiency may not be a robust signal for physiological drought stress detection, possibly due to variations of other environmental stresses or inaccurate characterization of the fluorescence efficiency. Although the EC sites are not evenly distributed across the study area, they represent the impact of drought on plant physiology for major biome types of the region. OCO-3 derived afternoon depression is strongly correlated with the depression of LUE calculated from EC (Pearson's r=.92, p<.001). Interestingly, we observe a weak relationship between the afternoon depression and the enhanced vegetation index (EVI, r=-.39, p=.69 for grassland, r=.22, p=.73 for shrubland), suggesting that the physiological stress development is decoupled from the vegetation greenness changes during this period. The OCO-3 SIF derived afternoon depressions occur earlier than the vegetation greenness declines, especially for grasslands, making this indicator a potential early warning signal for drought stress. VPD is expected to strongly affect the strength of the afternoon depression, and this is supported by a concurrent increase of the depression and VPD during February to August (Figure 3d). However, the relationship breaks down in the later period of the drought, likely due to a

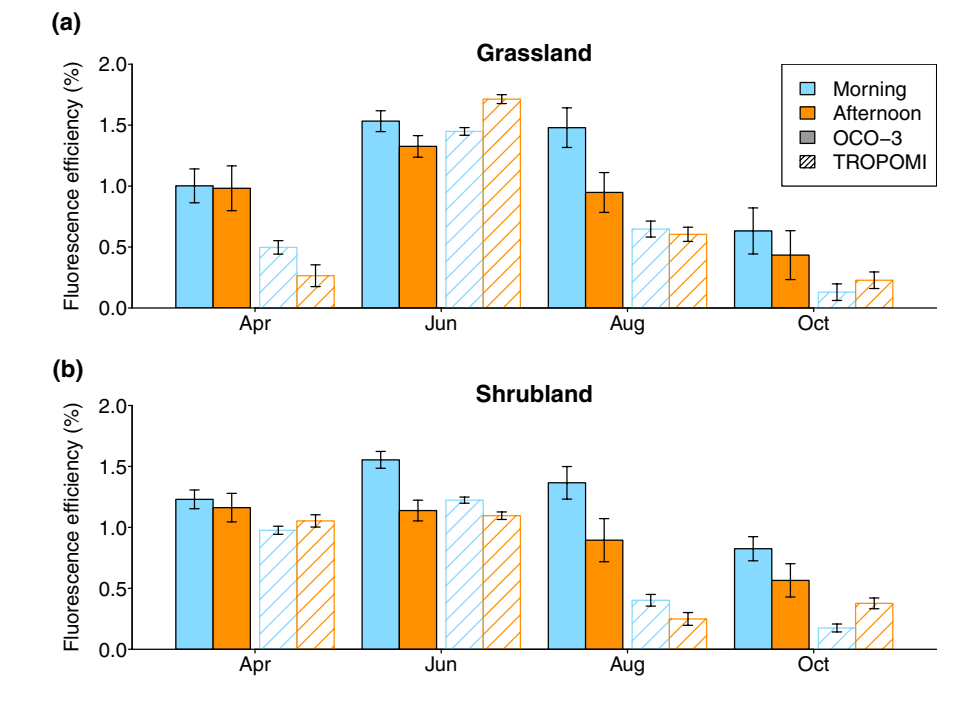
continuous decline of soil moisture that exacerbates stomatal sensitivity to VPD (Novick, Ficklin, et al., 2016). These results indicate that the OCO-3 observed afternoon depression of photosynthesis well captures the plant responses to the integrated physiological drought stress, which is independent from canopy greenness changes and cannot be represented by VPD, temperature or soil moisture alone.

To test if this satellite derived afternoon depression might be an artifact caused by differences in the sample locations, that is, whether the fluorescence efficiency happens to be higher for the OCO-3 morning sounding locations, and lower for the afternoon sounding locations, we calculated the fluorescence efficiency using the TROPOMI SIF for the corresponding sounding locations of OCO-3 SIF (SIF $_{\rm TROPOMI\text{-}OCO3}$). These $\rm SIF_{\rm TROPOMI\text{-}OCO3}$ observations can be categorized into morning and afternoon observations based on the corresponding OCO-3 overpass time. Since TROPOMI SIF observations are obtained around 13:30 local time and do not provide diurnal stress information, thus the fluorescence efficiency calculated from ${\rm SIF}_{\rm TROPOMI\text{-}OCO3}$ should not exhibit a difference between the OCO-3's morning sounding locations and afternoon sounding locations. Our analysis confirms this hypothesis by demonstrating that the calculated fluorescence efficiency is not systematically lower for afternoon (paired one-sided t-test, p = .57, Figure 4).

4.4 | Spatial mapping of plants physiological drought stress

The diurnal changes of physiological stress provide important information on how ecosystems respond to drought. To derive a spatially explicit map of diurnal physiological drought stress, we trained deep learning models based on OCO-3 SIF observations under non-drought conditions at different time of the day for grasslands and shrublands separately, and

FIGURE 4 Comparison between fluorescence yield calculated using morning and afternoon sample locations from OCO-3 and TROPOMI. Blue and red colors represent fluorescence yield for morning and afternoon, respectively. Solid and hatched bars represent results for OCO-3 and TROPOMI, respectively. Error bars show the 95% confidence intervals of the fluorescence yield estimates. For OCO-3, the samples are collected at different time of the day, while for TROPOMI, the samples are obtained from the same sounding locations as the OCO-3, with fixed observation time around 13:30. Only 4 months with enough samples are shown. (a) All grassland samples within each month. (b) All shrubland samples. [Colour figure can be viewed at wileyonlinelibrary.com]



use these models to predict a reference SIF during the drought period (Figure S3). The difference between observed SIF and predicted reference SIF (Δ SIF) can be interpreted as the physiological stress induced SIF reduction (Zhang, Joiner, et al., 2018). This approach also allows us to characterize the spatial patterns of the diurnal drought stress.

In April 2020 before the drought starts, ΔSIF is on average close to zero for the afternoon (Figure 5a). There is no obvious sign of afternoon depression when compared with morning and noon values (Figure 5d; Figure S16). As the drought stress develops, we observe a widespread signal of negative ΔSIF , corresponding to a strong afternoon depression for June and August. With the swath-based satellite

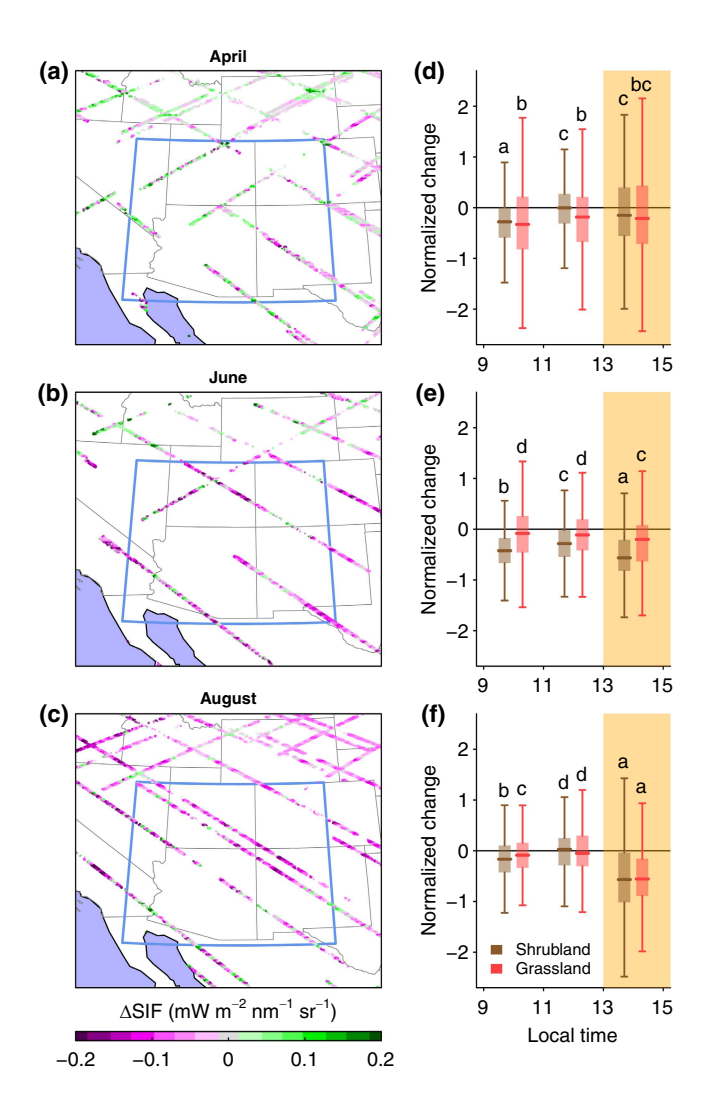


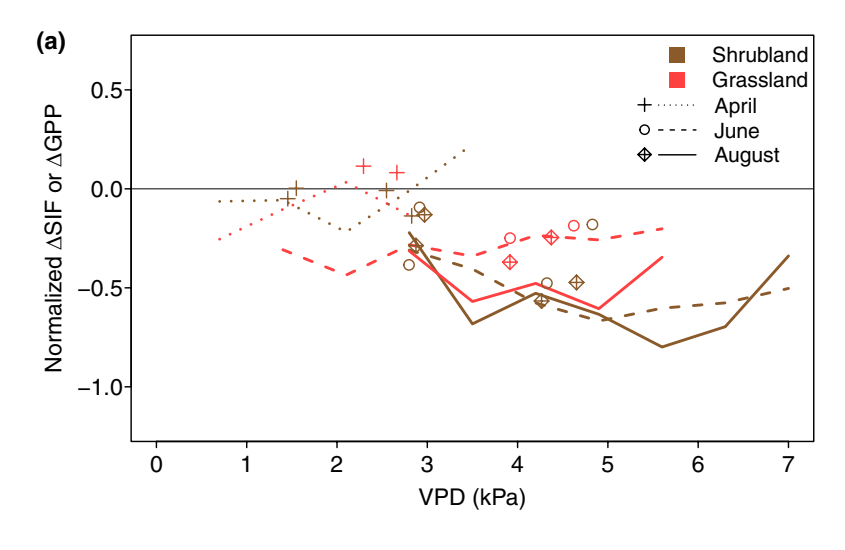
FIGURE 5 Spatial patterns of the afternoon depression. (a–c) Difference between observed SIF and machine learning predicted SIF (Δ SIF) in the afternoon (13:00 to 15:00) during the drought period. To reduce the noise of each SIF sounding, we calculate the average Δ SIF within the 0.1°×0.1° window for each sounding. (d–f) Boxplot of normalized Δ SIF for shrubland and grassland within the study area at different time of the day. Δ SIF is normalized by the regional mean of the predicted SIF for the study area (blue boundary) to account for the diurnal variation of radiation. Yellow shades indicate the period with strongest afternoon depression. Different letters indicate significant difference (p<.001) between groups. [Colour figure can be viewed at wileyonlinelibrary.com]

observations, we can assess the physiological drought stress spatially at ecosystem scale. For example, we find much weaker drought stress as indicated by a slight positive ΔSIF near the California-Arizona border (especially in June and August), where Colorado River can provide enough water for the local environment. Drought stress is also weaker in cooler mountainous regions in southern Colorado and western New Mexico (Figure 5b,c). These large diurnal variations of ΔSIF are not likely due to the model bias since we did not find such diurnal biases in the independent test and validation datasets (Figure S7).

Interestingly, satellite observations reveal different trajectories of physiological drought stress development between shrublands and grasslands. In April before the drought begins, afternoon depression signals are weak for both biomes (Figure 5d). The stress signals diverge as shrublands exhibit more negative afternoon ΔSIF in early drought period (June) while the depression is still relatively weak for grasslands (Figure 5e). Such a difference in emergence time of the stress signals may be partly attributed to a greater increase of VPD in shrublands (Figure 3c), but also to a stronger plants' sensitivity to VPD due to a lower soil moisture (Figure 6a; Novick, Ficklin, et al., 2016; Sperry et al., 2016). Declining soil water potential reduces plant hydraulic conductivity and xylem water transport, leading to a reduced transpiration and an increased stomatal sensitivity to VPD (Sperry et al., 2016). This biome-dependent depression-VPD relationship derived from satellite observations is also supported by independent EC measurements with high consistency (Pearson's r = .87, p < .001, Figure 6b). These analyses demonstrate that OCO-3, combined with other satellite observations, can spatially explicit map plants drought stress, which provide a valuable dataset to understand the mechanism of drought impact on plant physiology at large scale.

5 | DISCUSSION

In this study, we use two independent methods to demonstrate that the diurnal SIF observations from OCO-3 can be used to derive a robust signal of physiological drought stress. The observed afternoon depression of fluorescence efficiency and light use efficiency is likely caused by the high VPD-induced stomatal closure, which inhibit the light independent reaction of photosynthesis and feedback to the energy portioning of the light reaction (Porcar-Castell et al., 2014). Soil moisture and plant hydraulic traits also affect the water transport and regulate the stomatal sensitivity to VPD, further enhances the afternoon depressions as drought develops (Novick, Miniat, & Vose, 2016; Tuzet et al., 2003). Recent studies also suggest that chloroplast movements and leaf inclination in response to light and water stress can also partly explain the afternoon depression (Maai, 2020; Pastenes et al., 2005). These processes directly affect the plant water and carbon exchange at both diurnal and seasonal scales, but their effects are difficult to simulate at large scale using state-of-the-art DGVMs due to the limited observations for parameterizing the complex plant hydraulic module at large scale (Kennedy et al., 2019). The satelliteobserved afternoon depression can be used as an observational benchmark for both model parameterization and validation.



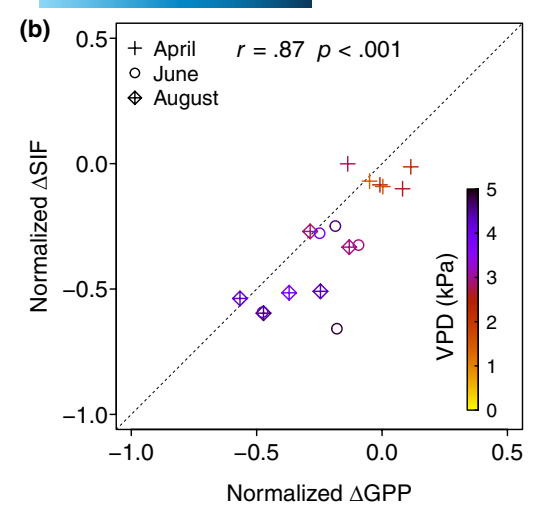


FIGURE 6 The vapor pressure deficit (VPD) effect on afternoon depression. (a) Effect size of afternoon depression along the VPD during the drought period. Lines indicate the average response of normalized afternoon depression of SIF (Δ SIF) within each VPD bin, with different line types indicate observations from different months. Points indicate afternoon depression of GPP (relative decrease of afternoon GPP to morning GPP) from EC observations. (b) Comparison between afternoon depression from OCO-3 (y-axis) and from EC (x-axis). Colors of the points indicate the monthly average VPD in the afternoon (13:00 to 15:00). [Colour figure can be viewed at wileyonlinelibrary.com]

In addition to SIF, a number of recently proposed vegetation indices have been shown to be robust proxies of terrestrial photosynthesis, for example, NIRv and its derivatives (Badgley et al., 2017; Dechant et al., 2022), kNDVI (Camps-Valls et al., 2021), but they largely represent canopy structural dynamics and do not provide information of drought stress on plant physiology (Magney et al., 2019; Martini et al., 2022). These indicators nevertheless show very strong spatiotemporal co-variation with SIF since fluorescence efficiency remains relatively stable during the non-stress period of the growing season (Dechant et al., 2020; Yang, Ryu, et al., 2018). Fluorescence efficiency becomes important when drought, heat or cold stress inhibit plant physiological processes (Kimm et al., 2021; Magney et al., 2019; Zeng et al., 2022). For example, fluorescence efficiency derived from in-situ SIF measurements at a temperature control experiment revealed a strong relationship with physiological stress (Kimm, Guan, Burroughs, et al., 2021). Recent studies indicate that satellite derived SIF has stronger sensitivity than conventional vegetation indices in response to drought (Smith et al., 2018), yet it remains unclear whether this advantage is contributed by the changes in plant physiology. By combining OCO-3 SIF and other satellite observations using radiative transfer modeling and machine learning, we are able to successfully derive the diurnal changes of fluorescence efficiency at the regional scale. This provides the first satellitebased evidence that SIF contains unique physiological information, especially at the diurnal time scale to track drought stress.

Although afternoon depression observed by satellite exhibits similar magnitude as that from EC, a linear photosynthesis-SIF relationship during drought is not warranted since the magnitude of average daily LUE decline may be different than that of fluorescence efficiency (Wieneke et al., 2018). In fact, recent studies based on site-level observations suggest that the strong

photosynthesis-SIF relationship breaks down during drought period (Martini et al., 2022). However, this satellite-retrieved signal can still play an important role in land surface modeling either serving as an empirical drought scalar or through model data fusion (Liu et al., 2020; Stocker et al., 2018). More importantly, this global observation provides new possibility in understanding how different ecosystems respond to drought physiologically. Due to the limited spatial coverage of the swath-based observations, OCO-3 cannot estimate drought stress contiguously across space. Geostationary Carbon Observatory (GEOCarb), NASA's new geostationary satellite set to launch in 2024, will provide hourly wall-to-wall mapping of SIF for North and South America (Somkuti et al., 2021), further enhancing our capability to monitor diurnal changes of physiological drought stress.

AUTHOR CONTRIBUTIONS

Yao Zhang designed the study; Yao Zhang and Jianing Fang performed the analysis; Yao Zhang wrote the manuscript. William Kolby Smith, Xian Wang, and Russell L. Scott, and Marcy Litvak contributed the site-level EC and SIF data. All co-authors commented on the results and contributed to the writing of the manuscript.

ACKNOWLEDGMENTS

Y.Z., and J.F. acknowledge support from the National Natural Science Foundation of China (42141005). W.K.S acknowledges support from the NASA Carbon Cycle Science Program (80NSSC23K0109). This work is supported by High-performance Computing Platform of Peking University. We thank Christian Frankenberg and Philipp Köhler for providing the OCO-3 dataset.

CONFLICT OF INTEREST STATEMENT

The authors declare no competing interests.



DATA AVAILABILITY STATEMENT

The OCO-3 SIF dataset is available at https://earthdata.nasa.gov/; the TROPOMI SIF dataset is available through ftp://fluo.gps.calte ch.edu/data/tropomi/; the CSIF dataset is available through https://doi.org/10.11888/Ecolo.tpdc.271751; the Ameriflux eddy covariance dataset is available through https://ameriflux.lbl.gov/data/download-data/; the MODIS MCD43A4, MYD11C1, and MCD12C2 data are available at https://earthdata.nasa.gov/; the ERA5 climate dataset is available at https://doi.org/10.24381/cds.adbb2d47; and the USDM drought classification is available at https://droughtmon itor.unl.edu/DmData/GISData.aspx.

CODE AVAILABILITY

All computer codes used in this study are available from the corresponding author upon reasonable request.

ORCID

Yao Zhang https://orcid.org/0000-0002-7468-2409
Xian Wang https://orcid.org/0000-0003-0018-2679
Sujong Jeong https://orcid.org/0000-0003-4586-4534
Marcy Litvak https://orcid.org/0000-0002-4255-2263

REFERENCES

- Adams, W. W., & Demmig-Adams, B. (2004). Chlorophyll fluorescence as a tool to monitor plant response to the environment. In *Chlorophyll a fluorescence*, *advances in photosynthesis and respiration* (pp. 583–604). Springer. https://doi.org/10.1007/978-1-4020-3218-9_22
- Allen, C. D., Macalady, A. K., Chenchouni, H., Bachelet, D., McDowell, N., Vennetier, M., Kitzberger, T., Rigling, A., Breshears, D. D., Hogg, E. T., Gonzalez, P., Fensham, R., Zhang, Z., Castro, J., Demidova, N., Lim, J., Allard, G., Running, S. W., Semerci, A., & Cobb, N. (2010). A global overview of drought and heat-induced tree mortality reveals emerging climate change risks for forests. Forest Ecology and Management, 259, 660–684. https://doi.org/10.1016/j.foreco.2009.09.001
- Anderegg, W. R. L., Kane, J. M., & Anderegg, L. D. L. (2013). Consequences of widespread tree mortality triggered by drought and temperature stress. *Nature Climate Change*, 3, 30–36. https://doi.org/10.1038/nclimate1635
- Badgley, G., Field, C. B., & Berry, J. A. (2017). Canopy near-infrared reflectance and terrestrial photosynthesis. *Science Advances*, 3, e1602244. https://doi.org/10.1126/sciadv.1602244
- Baker, N. R. (2008). Chlorophyll fluorescence: A probe of photosynthesis in vivo. *Annual Review of Plant Biology*, *59*, 89–113. https://doi.org/10.1146/annurev.arplant.59.032607.092759
- Camps-Valls, G., Campos-Taberner, M., Moreno-Martínez, Á., Walther, S., Duveiller, G., Cescatti, A., Mahecha, M. D., Muñoz-Marí, J., García-Haro, F. J., Guanter, L., Jung, M., Gamon, J. A., Reichstein, M., & Running, S. W. (2021). A unified vegetation index for quantifying the terrestrial biosphere. *Science Advances*, 7, eabc7447. https://doi.org/10.1126/sciadv.abc7447
- Chang, C. Y., Wen, J., Han, J., Kira, O., LeVonne, J., Melkonian, J., Riha, S. J., Skovira, J., Ng, S., Gu, L., Wood, J. D., Näthe, P., & Sun, Y. (2021). Unpacking the drivers of diurnal dynamics of sun-induced chlorophyll fluorescence (SIF): Canopy structure, plant physiology, instrument configuration and retrieval methods. *Remote Sensing of Environment*, 265, 112672. https://doi.org/10.1016/j.rse.2021.112672
- Ciais, P., Reichstein, M., Viovy, N., Granier, A., Ogée, J., Allard, V., Aubinet, M., Buchmann, N., Bernhofer, C., Carrara, A., Chevallier, F., De Noblet, N., Friend, A. D., Friedlingstein, P., Grünwald, T.,

- Heinesch, B., Keronen, P., Knohl, A., Krinner, G., ... Valentini, R. (2005). Europe-wide reduction in primary productivity caused by the heat and drought in 2003. *Nature*, 437, 529–533. https://doi.org/10.1038/nature03972
- Cowan, I. R., & Farquhar, G. D. (1977). Stomatal function in relation to leaf metabolism and environment. *Symposia of the Society for Experimental Biology*, *31*, 471–505.
- Dai, A. (2012). Increasing drought under global warming in observations and models. Nature Climate Change, 3, 52–58. https://doi. org/10.1038/nclimate1633
- Dannenberg, M. P., Yan, D., Barnes, M. L., Smith, W. K., Johnston, M. R., Scott, R. L., Biederman, J. A., Knowles, J. F., Wang, X., Duman, T., Litvak, M. E., Kimball, J. S., Williams, A. P., & Zhang, Y. (2022). Exceptional heat and atmospheric dryness amplified losses of primary production during the 2020 U.S. Southwest hot drought. Global Change Biology, 28, 4794–4806. https://doi.org/10.1111/gcb.16214
- Dechant, B., Ryu, Y., Badgley, G., Köhler, P., Rascher, U., Migliavacca, M., Zhang, Y., Tagliabue, G., Guan, K., Rossini, M., Goulas, Y., Zeng, Y., Frankenberg, C., & Berry, J. A. (2022). NIRVP: A robust structural proxy for sun-induced chlorophyll fluorescence and photosynthesis across scales. *Remote Sensing of Environment*, 268, 112763. https://doi.org/10.1016/j.rse.2021.112763
- Dechant, B., Ryu, Y., Badgley, G., Zeng, Y., Berry, J. A., Zhang, Y., Goulas, Y., Li, Z., Zhang, Q., Kang, M., Li, J., & Moya, I. (2020). Canopy structure explains the relationship between photosynthesis and sun-induced chlorophyll fluorescence in crops. *Remote Sensing of Environment*, 241, 111733. https://doi.org/10.1016/j.rse.2020.111733
- Eldering, A., Taylor, T. E., O'Dell, C. W., & Pavlick, R. (2019). The OCO-3 mission: Measurement objectives and expected performance based on 1 year of simulated data. *Atmospheric Measurement Techniques*, 12, 2341–2370. https://doi.org/10.5194/amt-12-2341-2019
- Franco, A., & Lüttge, U. (2002). Midday depression in savanna trees: Coordinated adjustments in photochemical efficiency, photorespiration, CO₂ assimilation and water use efficiency. *Oecologia*, 131, 356–365. https://doi.org/10.1007/s00442-002-0903-y
- Frankenberg, C., Fisher, J. B., Worden, J., Badgley, G., Saatchi, S. S., Lee, J. E., Toon, G. C., Butz, A., Jung, M., Kuze, A., & Yokota, T. (2011). New global observations of the terrestrial carbon cycle from GOSAT: Patterns of plant fluorescence with gross primary productivity. *Geophysical Research Letters*, 38, 1–6. https://doi.org/10.1029/2011GL048738
- Kennedy, D., Swenson, S., Oleson, K. W., Lawrence, D. M., Fisher, R., da Costa, A. C. L., & Gentine, P. (2019). Implementing plant hydraulics in the community land model, version 5. *Journal of Advances in Modeling Earth Systems*, 11, 485–513. https://doi.org/10.1029/2018MS001500
- Kimm, H., Guan, K., Burroughs, C. H., Peng, B., Ainsworth, E. A., Bernacchi, C. J., Moore, C. E., Kumagai, E., Yang, X., Berry, J. A., & Wu, G. (2021). Quantifying high-temperature stress on soybean canopy photosynthesis: The unique role of sun-induced chlorophyll fluorescence. *Global Change Biology*, *27*, 2403–2415. https://doi.org/10.1111/gcb.15603
- Kimm, H., Guan, K., Jiang, C., Miao, G., Wu, G., Suyker, A. E., Ainsworth, E. A., Bernacchi, C. J., Montes, C. M., Berry, J., Yang, X., Frankenberg, C., Chen, M., & Koehler, P. (2021). A physiological signal derived from sun-induced chlorophyll fluorescence quantifies crop physiological response to environmental stresses in the U.S. Corn Belt. Environmental Research Letters, 16. https://doi.org/10.1088/1748-9326/ac3b16
- Knowles, J. F., Scott, R. L., Minor, R. L., & Barron-Gafford, G. A. (2020). Ecosystem carbon and water cycling from a sky Island montane forest. Agricultural and Forest Meteorology, 281, 107835. https://doi. org/10.1016/j.agrformet.2019.107835
- Köhler, P., Frankenberg, C., Magney, T. S., Guanter, L., Joiner, J., & Landgraf, J. (2018). Global retrievals of solar-induced chlorophyll fluorescence with TROPOMI: First results and intersensor

) on Wiley Online Library for rules of use; OA articles are governed by the applicable Creative Commons

- comparison to OCO-2. Geophysical Research Letters, 45, 10456–10463. https://doi.org/10.1029/2018GL079031
- Lasslop, G., Reichstein, M., Papale, D., Richardson, A., Arneth, A., Barr, A., Stoy, P., & Wohlfahrt, G. (2010). Separation of net ecosystem exchange into assimilation and respiration using a light response curve approach: Critical issues and global evaluation. Global Change Biology, 16, 187–208. https://doi.org/10.1111/j.1365-2486. 2009.02041.x
- Lin, Y.-S., Medlyn, B. E., Duursma, R. A., Prentice, I. C., Wang, H., Baig, S., Eamus, D., de Dios, V. R., Mitchell, P., Ellsworth, D. S., de Beeck, M. O., Wallin, G., Uddling, J., Tarvainen, L., Linderson, M.-L., Cernusak, L. A., Nippert, J. B., Ocheltree, T. W., Tissue, D. T., ... Wingate, L. (2015). Optimal stomatal behaviour around the world. *Nature Climate Change*, 5, 459-464. https://doi.org/10.1038/nclimate2550
- Liu, Y., Kumar, M., Katul, G. G., Feng, X., & Konings, A. G. (2020). Plant hydraulics accentuates the effect of atmospheric moisture stress on transpiration. *Nature Climate Change*, 10, 691–695. https://doi.org/10.1038/s41558-020-0781-5
- Maai, E. (2020). Light stress-induced chloroplast movement and midday depression of photosynthesis in sorghum leaves. *Plant Production Science*, 23, 172–181.
- Magney, T. S., Bowling, D. R., Logan, B. A., Grossmann, K., Stutz, J., Blanken, P. D., Burns, S. P., Cheng, R., Garcia, M. A., Köhler, P., Lopez, S., Parazoo, N. C., Raczka, B., Schimel, D., & Frankenberg, C. (2019). Mechanistic evidence for tracking the seasonality of photosynthesis with solar-induced fluorescence. *Proceedings of the National Academy of Sciences of the United States of America*, 116, 11640–11645. https://doi.org/10.1073/pnas.1900278116
- Martens, B., Miralles, D. G., Lievens, H., van der Schalie, R., de Jeu, R. A. M., Fernández-Prieto, D., Beck, H. E., Dorigo, W. A., & Verhoest, N. E. C. (2017). GLEAM v3: Satellite-based land evaporation and root-zone soil moisture. Geoscientific Model Development, 10, 1903–1925. https://doi.org/10.5194/gmd-10-1903-2017
- Martini, D., Sakowska, K., Wohlfahrt, G., Pacheco-Labrador, J., van der Tol, C., Porcar-Castell, A., Magney, T. S., Carrara, A., Colombo, R., El-Madany, T. S., Gonzalez-Cascon, R., Martín, M. P., Julitta, T., Moreno, G., Rascher, U., Reichstein, M., Rossini, M., & Migliavacca, M. (2022). Heatwave breaks down the linearity between sun-induced fluorescence and gross primary production. *The New Phytologist*, 233, 2415– 2428. https://doi.org/10.1111/nph.17920
- Matthews, J. S. A., Vialet-Chabrand, S. R. M., & Lawson, T. (2017). Diurnal variation in gas exchange: The balance between carbon fixation and water loss. *Plant Physiology*, 174, 614–623. https://doi.org/10.1104/pp.17.00152
- McDowell, N. G., Sapes, G., Pivovaroff, A., Adams, H. D., Allen, C. D., Anderegg, W. R. L., Arend, M., Breshears, D. D., Brodribb, T., Choat, B., Cochard, H., De Cáceres, M., De Kauwe, M. G., Grossiord, C., Hammond, W. M., Hartmann, H., Hoch, G., Kahmen, A., Klein, T., ... Xu, C. (2022). Mechanisms of woody-plant mortality under rising drought, CO₂ and vapour pressure deficit. *Nature Reviews Earth & Environment*, 3, 294–308. https://doi.org/10.1038/s43017-022-00272-1
- Meroni, M., Busetto, L., Colombo, R., Guanter, L., Moreno, J., & Verhoef, W. (2010). Performance of spectral fitting methods for vegetation fluorescence quantification. *Remote Sensing of Environment*, 114, 363–374. https://doi.org/10.1016/j.rse.2009.09.010
- Novick, K. A., Ficklin, D. L., Stoy, P. C., Williams, C. A., Bohrer, G., Oishi, A. C., Papuga, S. A., Blanken, P. D., Noormets, A., Sulman, B. N., Scott, R. L., Wang, L., & Phillips, R. P. (2016). The increasing importance of atmospheric demand for ecosystem water and carbon fluxes. Nature Climate Change, 6, 1023–1027. https://doi.org/10.1038/nclimate3114
- Novick, K. A., Miniat, C. F., & Vose, J. M. (2016). Drought limitations to leaf-level gas exchange: Results from a model linking stomatal optimization and cohesion-tension theory. *Plant, Cell & Environment, 39*, 583–596. https://doi.org/10.1111/pce.12657

- Pastenes, C., Pimentel, P., & Lillo, J. (2005). Leaf movements and photoinhibition in relation to water stress in field-grown beans. *Journal of Experimental Botany*, 56, 425–433. https://doi.org/10.1093/jxb/eri061
- Porcar-Castell, A., Malenovský, Z., Magney, T., Van Wittenberghe, S., Fernández-Marín, B., Maignan, F., Zhang, Y., Maseyk, K., Atherton, J., Albert, L. P., Robson, T. M., Zhao, F., Garcia-Plazaola, J.-I., Ensminger, I., Rajewicz, P. A., Grebe, S., Tikkanen, M., Kellner, J. R., Ihalainen, J. A., ... Logan, B. (2021). Chlorophyll a fluorescence illuminates a path connecting plant molecular biology to Earth-system science. *Nature Plants*. https://doi.org/10.1038/s41477-021-00980-4
- Porcar-Castell, A., Tyystjärvi, E., Atherton, J., Van Der Tol, C., Flexas, J., Pfündel, E. E., Moreno, J., Frankenberg, C., & Berry, J. A. (2014). Linking chlorophyll a fluorescence to photosynthesis for remote sensing applications: Mechanisms and challenges. *Journal of Experimental Botany*, 65, 4065–4095. https://doi.org/10.1093/jxb/eru191
- Reichstein, M., Falge, E., Baldocchi, D., Papale, D., Aubinet, M., Berbigier, P., Bernhofer, C., Buchmann, N., Gilmanov, T., Granier, A., Grünwald, T., Havránková, K., Ilvesniemi, H., Janous, D., Knohl, A., Laurila, T., Lohila, A., Loustau, D., Matteucci, G., ... Valentini, R. (2005). On the separation of net ecosystem exchange into assimilation and ecosystem respiration: Review and improved algorithm. Global Change Biology, 11, 1424–1439. https://doi.org/10.1111/j.1365-2486.2005.001002.x
- Schaaf, C., & Wang, Z. (2015). MCD43A4 MODIS/Terra+Aqua BRDF/ Albedo Nadir BRDF Adjusted Ref Daily L3 Global-500m V006. https://doi.org/10.5067/MODIS/MCD43A4.006
- Scott, R. L., Hamerlynck, E. P., Jenerette, G. D., Moran, M. S., & Barron-Gafford, G. A. (2010). Carbon dioxide exchange in a semidesert grassland through drought-induced vegetation change. *Journal of Geophysical Research: Biogeosciences*, 115, 1–12. https://doi.org/10.1029/2010JG001348
- Smith, W. K., Biederman, J. A., Scott, R. L., Moore, D. J. P., He, M., Kimball, J. S., Yan, D., Hudson, A., Barnes, M. L., MacBean, N., Fox, A. M., & Litvak, M. E. (2018). Chlorophyll fluorescence better captures seasonal and interannual gross primary productivity dynamics across dryland ecosystems of southwestern North America. *Geophysical Research Letters*, 45, 748–757. https://doi.org/10.1002/2017GL075922
- Somkuti, P., O'Dell, C. W., Crowell, S., Köhler, P., McGarragh, G. R., Cronk, H. Q., & Burgh, E. B. (2021). Solar-induced chlorophyll fluorescence from the Geostationary Carbon Cycle Observatory (GeoCarb): An extensive simulation study. *Remote Sensing of Environment*, 263, 112565. https://doi.org/10.1016/j.rse.2021.112565
- Sperry, J. S., Wang, Y., Wolfe, B. T., Mackay, D. S., Anderegg, W. R. L., McDowell, N. G., & Pockman, W. T. (2016). Pragmatic hydraulic theory predicts stomatal responses to climatic water deficits. *The New Phytologist*, 212, 577–589. https://doi.org/10.1111/nph.14059
- Stocker, B. D., Zscheischler, J., Keenan, T. F., Prentice, I. C., Peñuelas, J., & Seneviratne, S. I. (2018). Quantifying soil moisture impacts on light use efficiency across biomes. *The New Phytologist*, 218, 1430–1449. https://doi.org/10.1111/nph.15123
- Stocker, B. D., Zscheischler, J., Keenan, T. F., Prentice, I. C., Seneviratne, S. I., & Peñuelas, J. (2019). Drought impacts on terrestrial primary production underestimated by satellite monitoring. *Nature Geoscience*, 12, 264–270. https://doi.org/10.1038/s41561-019-0318-6
- Sun, Y., Frankenberg, C., Jung, M., Joiner, J., Guanter, L., Köhler, P., & Magney, T. (2018). Overview of solar-induced chlorophyll fluorescence (SIF) from the orbiting carbon Observatory-2: Retrieval, cross-mission comparison, and global monitoring for GPP. Remote Sensing of Environment, 209, 808–823. https://doi.org/10.1016/j.rse.2018.02.016
- Taylor, T. E., Eldering, A., Merrelli, A., Kiel, M., Somkuti, P., Cheng, C., Rosenberg, R., Fisher, B., Crisp, D., Basilio, R., Bennett, M., Cervantes, D., Chang, A., Dang, L., Frankenberg, C., Haemmerle, V. R., Keller, G. R., Kurosu, T., Laughner, J. L., ... Yu, S. (2020). OCO-3 early mission operations and initial (vEarly) XCO2 and SIF

- retrievals. Remote Sensing of Environment, 251, 112032. https://doi.org/10.1016/j.rse.2020.112032
- Trugman, A. T., Medvigy, D., Mankin, J. S., & Anderegg, W. R. L. (2018). Soil moisture stress as a major driver of carbon cycle uncertainty. *Geophysical Research Letters*, 45, 6495–6503. https://doi.org/10.1029/2018GL078131
- Tuzet, A., Perrier, A., & Leuning, R. (2003). A coupled model of stomatal conductance, photosynthesis and transpiration. *Plant, Cell & Environment*, 26, 1097–1116. https://doi.org/10.1046/j.1365-3040.2003.01035.x
- vander Tol, C., Berry, J. A., Campbell, P. K. E., & Rascher, U. (2014). Models of fluorescence and photosynthesis for interpreting measurements of solar-induced chlorophyll fluorescence. *Journal of Geophysical Research: Biogeosciences*, 119, 2312–2327. https://doi.org/10.1002/2014JG002713
- Wieneke, S., Burkart, A., Cendrero-Mateo, M. P., Julitta, T., Rossini, M., Schickling, A., Schmidt, M., & Rascher, U. (2018). Linking photosynthesis and sun-induced fluorescence at sub-daily to seasonal scales. *Remote Sensing of Environment*, 219, 247–258. https://doi.org/10.1016/j.rse.2018.10.019
- Wutzler, T., Lucas-Moffat, A., Migliavacca, M., Knauer, J., Sickel, K., Šigut, L., Menzer, O., & Reichstein, M. (2018). Basic and extensible post-processing of eddy covariance flux data with REddyProc. *Biogeosciences*, 15, 5015–5030. https://doi.org/10.5194/bg-15-5015-2018
- Xiao, J., Fisher, J. B., Hashimoto, H., Ichii, K., & Parazoo, N. C. (2021). Emerging satellite observations for diurnal cycling of ecosystem processes. *Nature Plants*, 7, 877–887. https://doi.org/10.1038/ s41477-021-00952-8
- Yang, K., Ryu, Y., Dechant, B., Berry, J. A., Hwang, Y., Jiang, C., Kang, M., Kim, J., Kimm, H., Kornfeld, A., & Yang, X. (2018). Sun-induced chlorophyll fluorescence is more strongly related to absorbed light than to photosynthesis at half-hourly resolution in a rice paddy. *Remote Sensing of Environment*, 216, 658–673. https://doi.org/10.1016/j.rse.2018.07.008
- Yang, P., & van der Tol, C. (2018). Linking canopy scattering of far-red sun-induced chlorophyll fluorescence with reflectance. Remote Sensing of Environment, 209, 456–467. https://doi.org/10.1016/j. rse.2018.02.029
- Yang, X., Shi, H., Stovall, A., Guan, K., Miao, G., Zhang, Y., Zhang, Y., Xiao, X., Ryu, Y., & Lee, J.-E. (2018). FluoSpec 2—An automated field spectroscopy system to monitor canopy solar-induced fluorescence. Sensors, 18, 2063. https://doi.org/10.3390/s18072063
- Zeng, Y., Badgley, G., Dechant, B., Ryu, Y., Chen, M., & Berry, J. A. (2019). A practical approach for estimating the escape ratio of near-infrared solar-induced chlorophyll fluorescence. *Remote Sensing of Environment*, 232, 111209. https://doi.org/10.1016/j.rse.2019.05.028
- Zeng, Y., Chen, M., Hao, D., Damm, A., Badgley, G., Rascher, U., Johnson, J. E., Dechant, B., Siegmann, B., Ryu, Y., Qiu, H., Krieger,

- V., Panigada, C., Celesti, M., Miglietta, F., Yang, X., & Berry, J. A. (2022). Combining near-infrared radiance of vegetation and fluorescence spectroscopy to detect effects of abiotic changes and stresses. *Remote Sensing of Environment*, 270, 112856. https://doi.org/10.1016/j.rse.2021.112856
- Zhang, Y., Joiner, J., Alemohammad, S. H., Zhou, S., & Gentine, P. (2018). A global spatially contiguous solar-induced fluorescence (CSIF) dataset using neural networks. *Biogeosciences*, 15, 5779–5800. https://doi.org/10.5194/bg-15-5779-2018
- Zhang, Y., Keenan, T. F., & Zhou, S. (2021). Exacerbated drought impacts on global ecosystems due to structural overshoot. *Nature Ecology & Evolution*, 5, 1490–1498. https://doi.org/10.1038/s41559-021-01551-8
- Zhang, Y., Xiao, X., Zhou, S., Ciais, P., McCarthy, H., & Luo, Y. (2016). Canopy and physiological controls of GPP during drought and heat wave. *Geophysical Research Letters*, 43, 2016GL068501. https://doi. org/10.1002/2016GL068501
- Zhang, Z., & Zhang, Y. (2023). Solar angle matters: Diurnal pattern of solar-induced chlorophyll fluorescence from OCO-3 and TROPOMI. Remote Sensing of Environment, 285, 113380. https://doi.org/10.1016/j.rse.2022.113380
- Zhang, Z., Zhang, Y., Joiner, J., & Migliavacca, M. (2018). Angle matters: Bidirectional effects impact the slope of relationship between gross primary productivity and sun-induced chlorophyll fluorescence from Orbiting Carbon Observatory-2 across biomes. Global Change Biology, 24, 5017–5020. https://doi.org/10.1111/gcb.14427
- Zhou, S., Yu, B., Huang, Y., & Wang, G. (2014). The effect of vapor pressure deficit on water use efficiency at the subdaily time scale. *Geophysical Research Letters*, 41, 5005–5013. https://doi.org/10.1002/2014GL060741

SUPPORTING INFORMATION

Additional supporting information can be found online in the Supporting Information section at the end of this article.

How to cite this article: Zhang, Y., Fang, J., Smith, W. K., Wang, X., Gentine, P., Scott, R. L., Migliavacca, M., Jeong, S., Litvak, M., & Zhou, S. (2023). Satellite solar-induced chlorophyll fluorescence tracks physiological drought stress development during 2020 southwest US drought. *Global Change Biology*, *29*, 3395–3408. https://doi.org/10.1111/gcb.16683